JOURNAL OF MATERIALS SCIENCE **36** (2001) 5093–5100

High resolution TEM study of ceramic $BaO{\cdot}Pr_2O_3{\cdot}4TiO_2$

F. AZOUGH
Materials Science Centre, University of Manchester/UMIST, Grosvenor Street, Manchester, M1 7HS, UK

A. C. WRIGHT
Advanced Materials Research Laboratory, North East Wales Institute of Higher Education, Mold Road, Wrexham LLII 2LW, UK

R. FREER
Materials Science Centre, University of Manchester/UMIST, Grosvenor Street, Manchester, M1 7HS, UK
E-mail: robert.freer@umist.ac.uk

Ceramic specimens of $BaO{\cdot}Pr_2O_3{\cdot}4TiO_2$ ($Ba_{4.5}Pr_9Ti_{18}O_{54}$) were prepared by the mixed oxide-route. The single phase products were examined by High Resolution Transmission Electron Microscopy (HRTEM). Orthorhombic symmetry, with cell parameters $a \sim 22.2$ Å, $b \sim 12.2$ Å and $c \sim 7.6$ Å, was confirmed. On the basis of space group *pnam* (No. 62) and the crystal structural data of Rawn *et al.*, good agreement was obtained between the experimental HRTEM images and images simulated by the multislice method.

1. Introduction

Dielectric ceramics in the system $Ba_{6-3x}Ln_{8+2x}Ti_{18}O_{54}$ exhibit high dielectric constant ($\varepsilon_r = 80$–100), low loss (Qxf = 6000–9000) and dielectric properties that are stable with respect to temperature; These properties make the ceramics suitable for electronic applications, particularly at microwave frequencies [1–7]. The compound $BaO{\cdot}Pr_2O_3{\cdot}4TiO_2$ is a member of this solid solution family. There are a number structural models [2, 7–14] for the system and although these various models differ in their detail, there is consensus that the crystal structure belongs to the tungsten bronze structure family and essentially consists of a three dimensional framework of corner-sharing perovskite-like TiO_6 octahedra joined according to a pattern similar to that of tungsten-bronze.

Gens *et al*. [8] were the first to suggest possible space groups for the solid solution phases. Based on the systematic absences observed in single crystal electron diffraction patterns of $BaO{\cdot}La_2O_3{\cdot}4TiO_2$, they reported the probable space groups as pba2 (No. 32) or pbam (No. 55). Matveeva *et al*. [9] later confirmed these results by single-crystal X-ray diffraction and X-ray spectroscopic studies of single crystal $Ba_{4.5}Pr_9Ti_{18}O_{54}$, reporting the same space groups. Based on data for 1990 measured peaks, Matveeva *et al*. [9] calculated atomic positions using space group pba2. Approximately 400 additional peaks, corresponding to a doubling of the period along the *z* direction were also identified, but omitted from the crystal refinement. A similar model was subsequently proposed by Roth *et al*. [10]. Ohsato *et al*. [12] also detected superlattice X-ray diffraction peaks in studies of $Ba_{3.75}Pr_{9.5}Ti_{18}O_{54}$ crystals and reported an orthorhombic lattice. The space group of their fundamental lattice agreed with that of Matveeva *et al*., but that of the doubled cell was reported to be either $pbn2_1$ (No. 33) or pbnm (No. 62). By the use of X-ray diffraction methods Kolar [7] confirmed the findings of Matveeva *et al*. [9].

Azough *et al*. [1] studied $Ba_{4.5}Pr_9Ti_{18}O_{54}$ ceramic by electron diffraction. By observing systematic absences in microdiffraction patterns, they also determined the space group to be either $pna2_1$ (No. 33) or pnam (No. 62). Since these two space groups have different point symmetries, convergent-beam electron diffraction (CBED) parallel to [100] was used to distinguish between them. They concluded that the observed 2 mm symmetry of the zero-order Laue zone (ZOLZ) and the whole pattern confirmed that the space group must be pnam (No. 62). Ubic *et al*. [15] investigated the Nd- analogue of the solid solution in polycrystalline form by electron diffraction. They observed weak extra reflections in electron diffraction patterns, possibly due to small breaks in symmetry, and therefore suggested that the space group may be pb21m (No. 26). However, these weak extra reflections may arise from double diffraction. Rawn [13], performed Rietveld analysis of powder X-ray diffraction data of $Ba_{4.5}Ln_9Ti_{18}O_{54}$ (Ln = La and Gd) and determined the space groups to be $pba2_1$ (No. 33) for the La analogue and pnma (No. 62) for the Gd analogue. Rawn *et al*. [2] subsequently reported the atomic

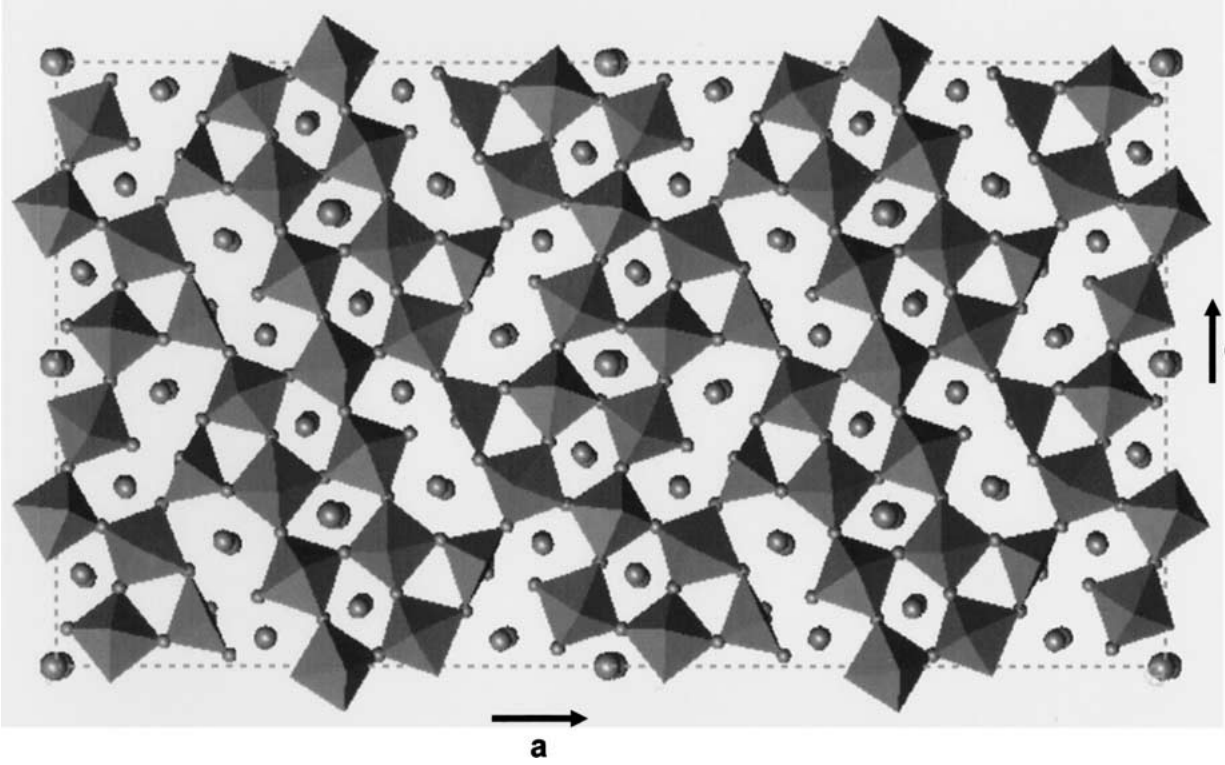

Figure 1 Schematic representation of the crystal structure of $Ba_{(6-2x)}Sm_{(8+2x)}Ti_{18}O_{54}$ ($x = 0.27$) according to Rawn *et al*. [2].

positions for $Ba_{(6-3x)}Sm_{(8+2x)}Ti_{18}O_{54}$ ($x = 0.27$ using space group pnma (No. 62). The schematic representation of the structure proposed by Rawn *et al*. [2]. is shown in Fig. 1. Between the network formed by the corner-sharing Ti-octahedra are three types of channels, pentagonal, tetragonal and triangular. In general, rare earth ions occupy the rhombic channels, Ba ions fill the pentagonal channels and the remaining Ba ions share the rhombic channels. The triangular channels are empty [16].

Based on the atomic positions reported by Rawn *et al*. [2] and the space group pnam deduced by Azough *et al*. [1] we have simulated TEM images for $Ba_{4.5}Pr_9Ti_{18}O_{54}$ by the multislice method and compared results with experimental images.

2. Experimental procedures

Ceramic samples were made by the mixed oxide-route. Powders of $BaCO_3$, Pr_6O_{11}, and TiO_2 (Fluka Chemicals, England) were mixed in the required proportions and wet milled for 12 hours. The mixture was calcined at 1100°C for 4 hours and wet milled again for 12 hours. After drying, the powders were pressed (uniaxially) into discs of 16 mm diameter, sintered in air in the temperature range 1350°C to 1450°C and cooled at a rate of 120 C h^{-1}. Products were examined by X-ray powder diffraction using Cu K_α radiation (Philips PW 1800 with horizontal goniometer). Scanning electron microscopy with energy dispersive spectroscopy (Philips 505 with EDAX) was used to assess sample homogeneity. For transmission electron microscopy (TEM) samples were prepared in two ways: (i) discs of ceramic were thinned mechanically and then ion beam thinned (ION TEC, TEC 791), or (ii) pellets were crushed and ground in an agate mortar and pestle. For the latter, particles were deposited on a carbon coated copper grid. A Phillips EM430 Transmission Electron Microscope was used for lattice imaging and electron diffraction studies. Lattice images were obtained at an accelerating voltage of 300 keV by the Many Beam Imaging (MBI) method. In order to interpret the high resolution images, image simulations were prepared by the multislice method [17] using the HRTEM module of the Cerius2 package of MSI Inc. (ver. 3.0) which is an implementation of the well-known multislice technique [17]. For the [010] zone, Fourier coefficients out to 0.4 nm (96 by 192 'beams') were included to generate a sequential set of three different projected potentials each with a slice thickness of 0.255 nm. The multislice iteration retained beam indexes out to 10 by 17 within the internal 'aperture' of the algorithm. No absorption potentials were included in the calculation. Images were calculated over a range of crystal thickness (integral multiples of the crystal unit cell only) and range of defocus (0 to –110 nm) for comparison with the experimental data; a combination of manufacturer's data for the EM430 TEM, i.e. spherical aberration coefficient, $C_s = 1.2$ mm, experimental data for beam convergence (0.7 mrad) and calculated focus spread (10 nm) were employed in the simulation. Beam convergence and focal spread effects were approximated using the mutual transfer function rather than by image averaging. An objective aperture size of 0.075 nm^{-1} was used.

3. Results and discussion

X-ray diffraction and SEM analyses confirmed that the samples were single phase with the expected composition.

Selected area diffraction patterns (SADP) studies confirmed the orthorhombic crystal structure.

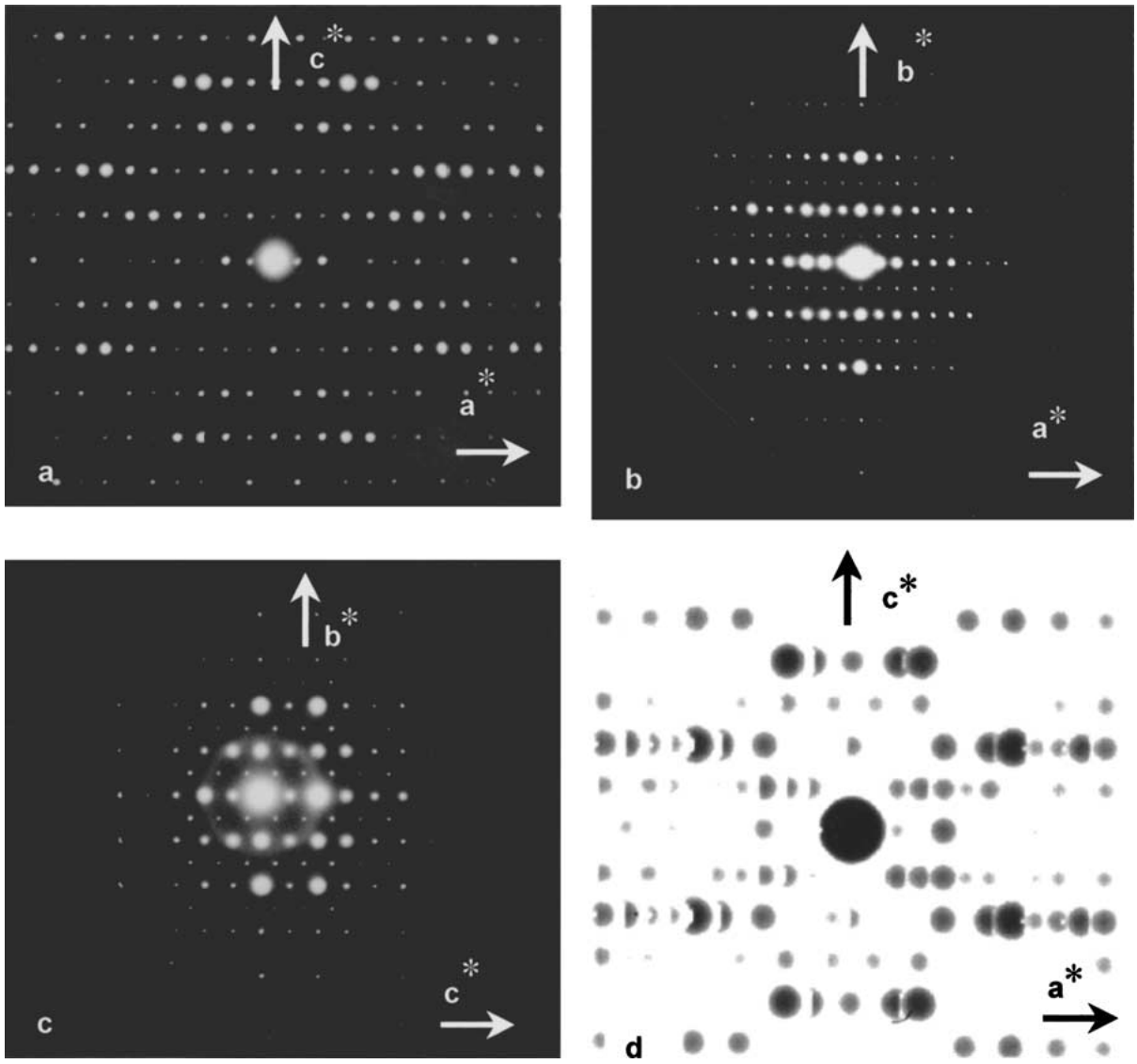

Figure 2 (a,b,a) experimental electron diffraction patterns along [010], [001] and [100] respectively; (d) simulated diffraction pattern for [010] orientation.

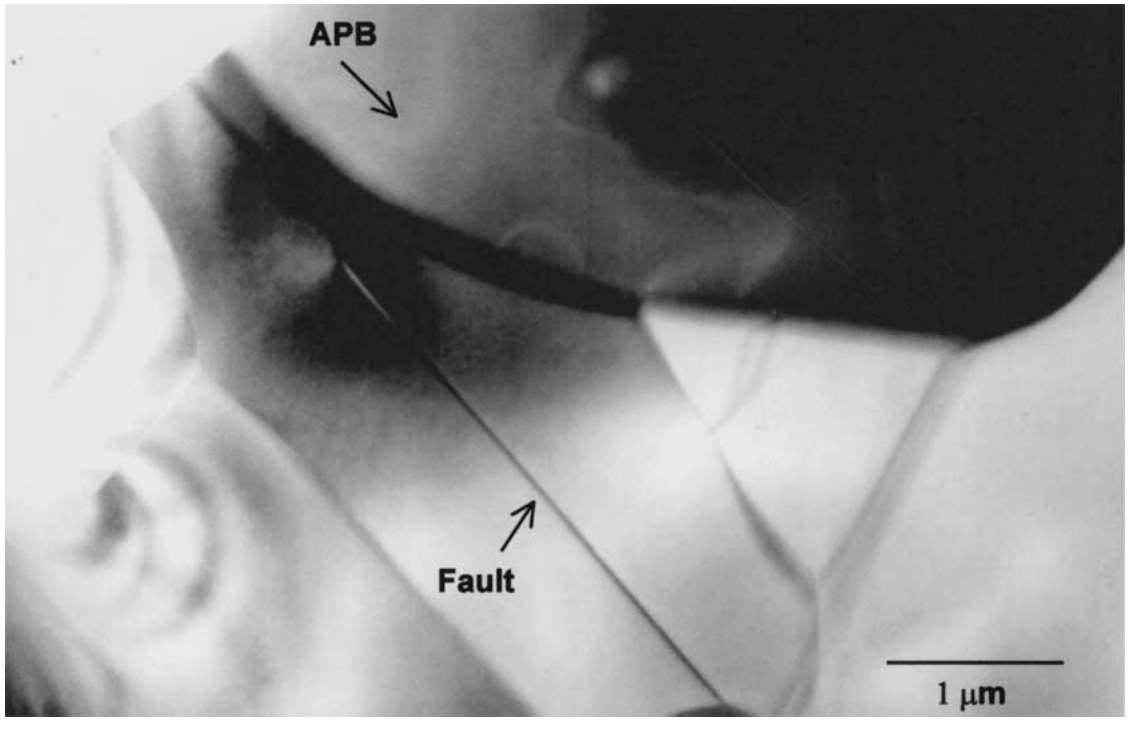

Figure 3 TEM image showing the presence of anti-phase domain boundary and a planar fault.

Fig. 2a,b,c shows electron diffraction patterns obtained for directions parallel to the three main crystallographic axes. The calculated lattice parameters are $a \sim 22.2$ Å, $b \sim 7.6$ Å and $c \sim 12.2$ Å. The simulated diffraction pattern for the [010] orientation is presented in Fig. 2d; there is good agreement with the experimental diffraction pattern (Fig. 2a).

A low magnification TEM image of the ceramic is shown in Fig. 3. No second phase was observed and EDS analysis of individual grains confirmed sample homogeneity. Two features were observed in the grain shown in Fig. 3; a planar fault running across the grain and anti-phase domain boundaries. The presence of the anti-phase domain boundaries (APB's) indicates the occurrence of an order-disorder transformation. The latter arises by a nucleation and growth mechanism, and causes the doubling of the shortest axis. Details of the planar fault are shown in Fig. 4. It can be seen that the

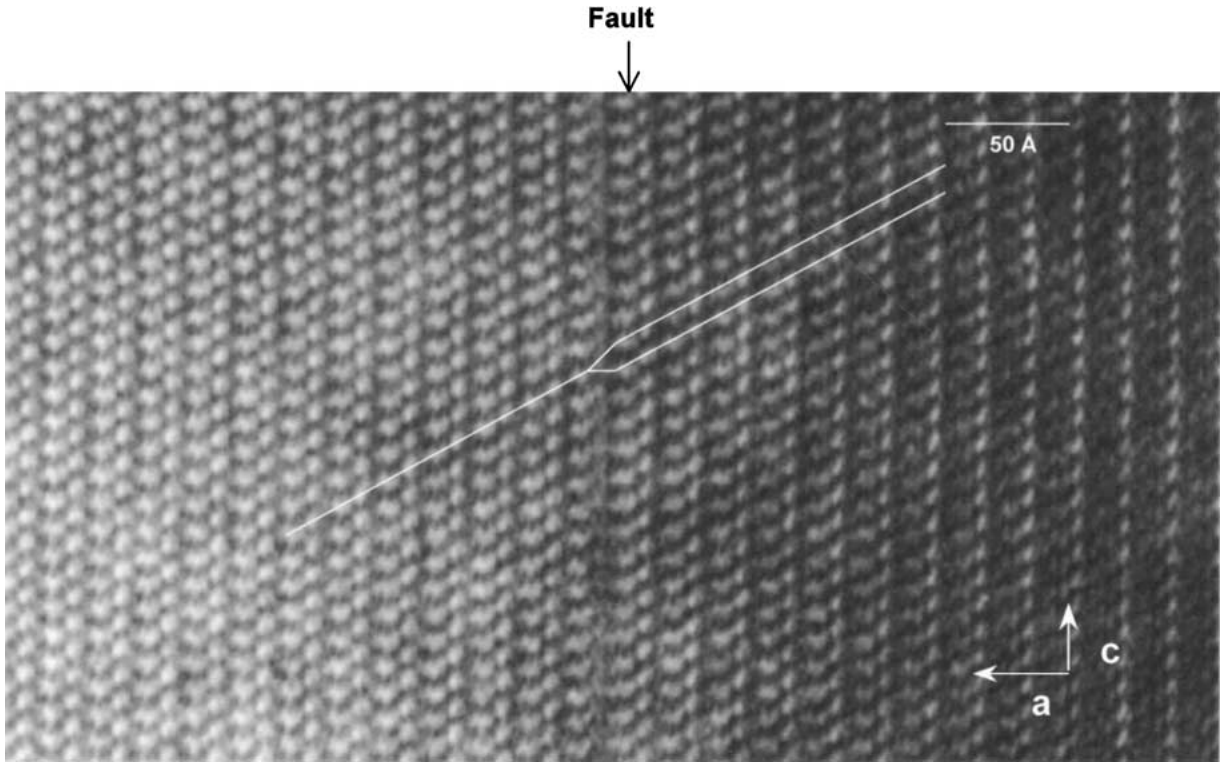

Figure 4 HRTEM image of the planar fault (Fig. 3) showing a displacement vector of $c/2$.

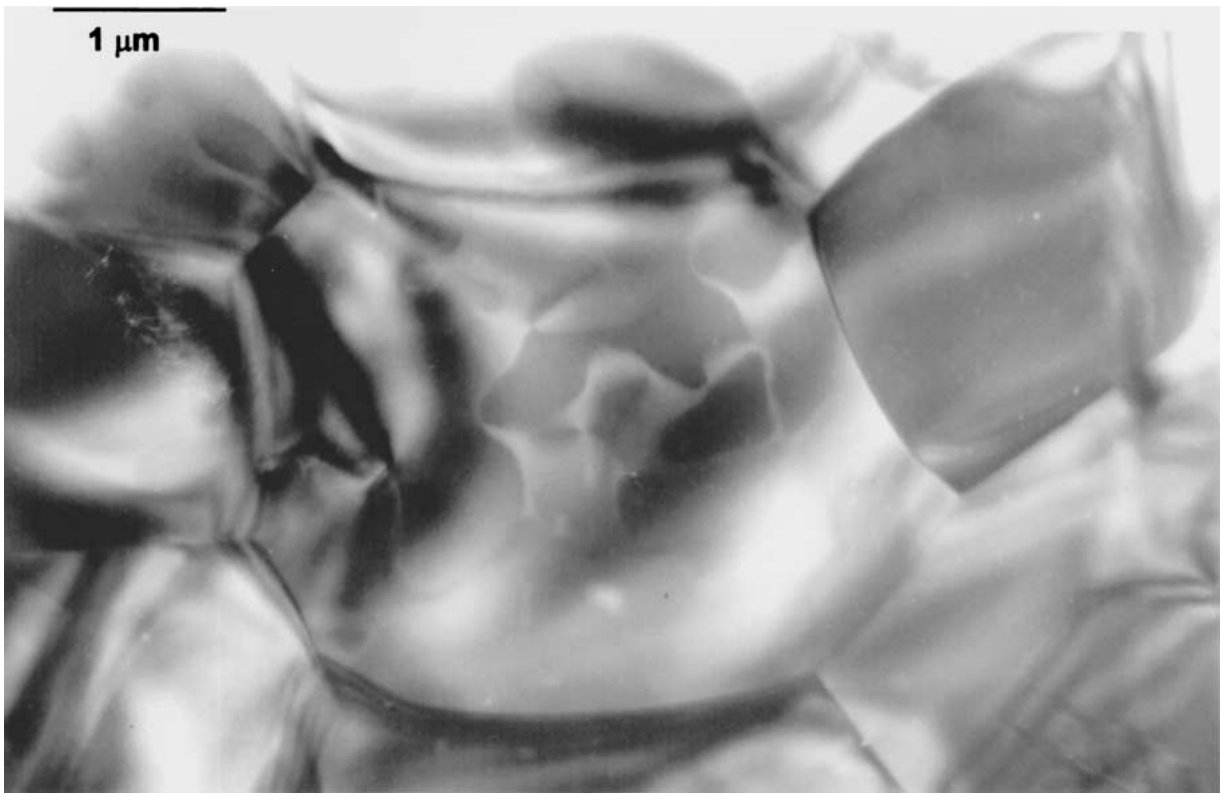

Figure 5 TEM image showing anti-phase boundaries.

fault (possibly an order-disorder transformation twin) has a displacement vector of $c/2$. Fig. 5 is a higher magnification TEM image of a grain showing anti-phase domain boundaries. Using darkfield imaging we have deduced that these anti-phase domains have a displacement vector $b/2$ [1].

Fig. 6a,b,c shows experimental HRTEM images of the ceramic for [010], [001] and [100] orientations. The experimental images were taken close to the Scherzer setting (−735 Å for the instrument). This was achieved via knowledge of both the step size (60 Å) and the number of steps away from the minimum contrast at the specimen edge. These images enable the octahedral chains (Fig. 6b and c) and the cavities (Fig. 6a) to be viewed.

Detailed simulation studies concentrated on the [010] orientation, containing Ti-octahedra, and the pentagonal and rhombic channels (occupied by Ba and Pr). The simulated images for [010] orientation at two thickness of unit cell, i.e. one cell (7.56 Å) and 7 unit cell (53.4 Å), are shown in Fig. 7a,b in the defocus range of −400 Å to −800 Å. For both thicknesses there is a good match with the experimental image (Fig. 6a). The best match is for the thickness of 1 unit cell in the defocus range −600 Å to −800 Å. This defocus range includes the Sherzer setting at which the experimental image was obtained.

A simulated projected potential, showing electron densities, for $Ba_{4.5}Pr_9Ti_{18}O_{54}$ along [010] is presented in Fig. 8. The unit cell is outlined and the positions of ions are marked.

The experimental image for the [010] direction (from Fig. 6a) and the corresponding simulated image for a thin crystal (Fig. 7b, –700 Å) can be compared with the

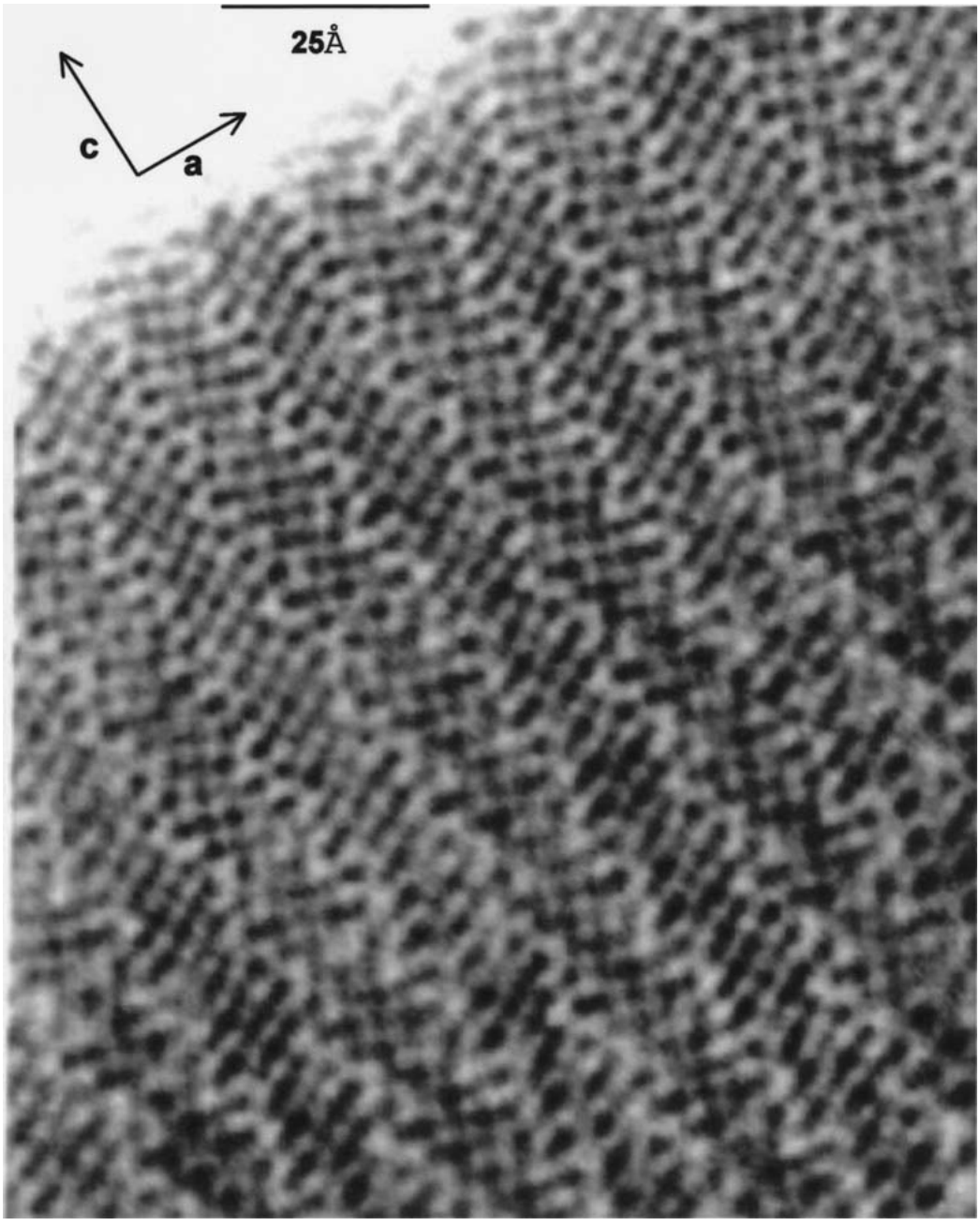

(a)

Figure 6 (a,b,c) HRTEM images for [010], [001] and [100] orientation respectively. *(Continued.)*

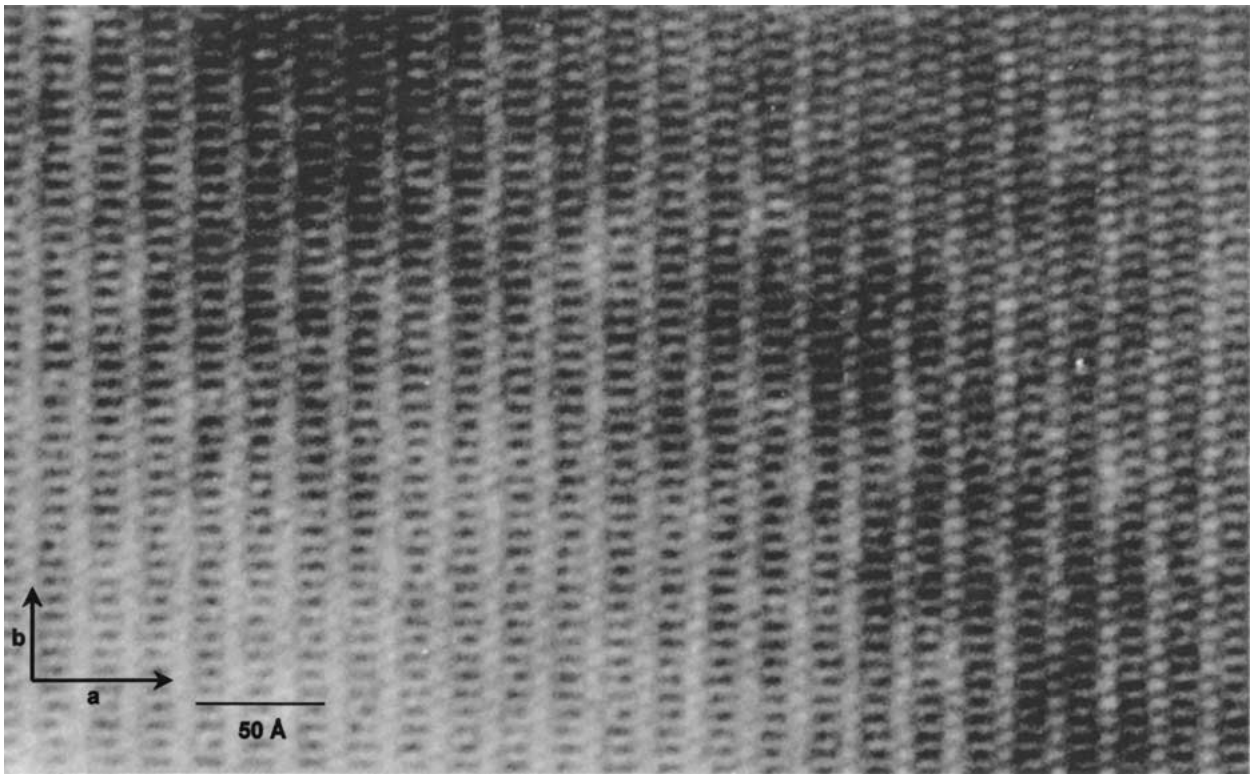

(b)

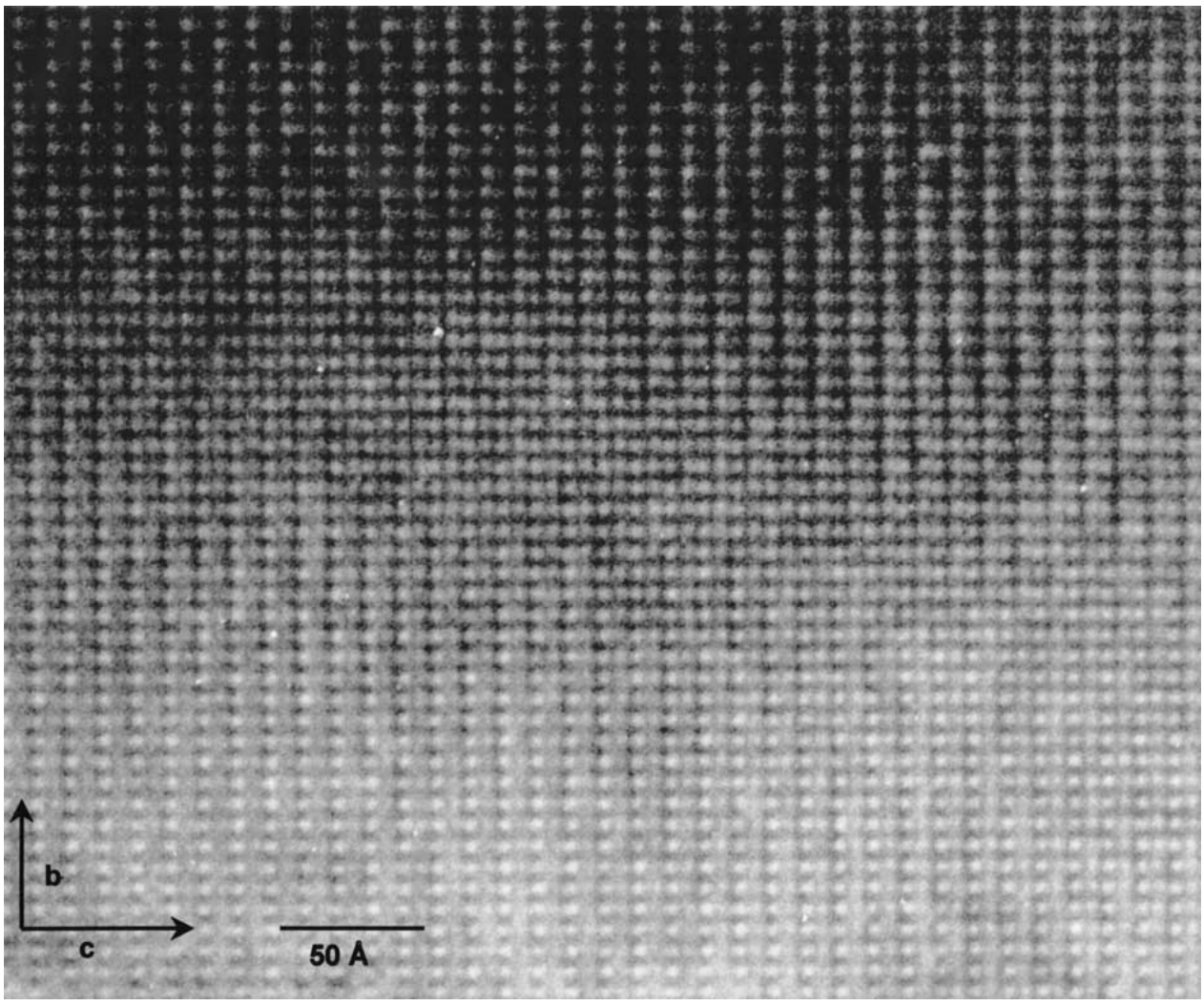

(c)

Figure 6 (Continued.)

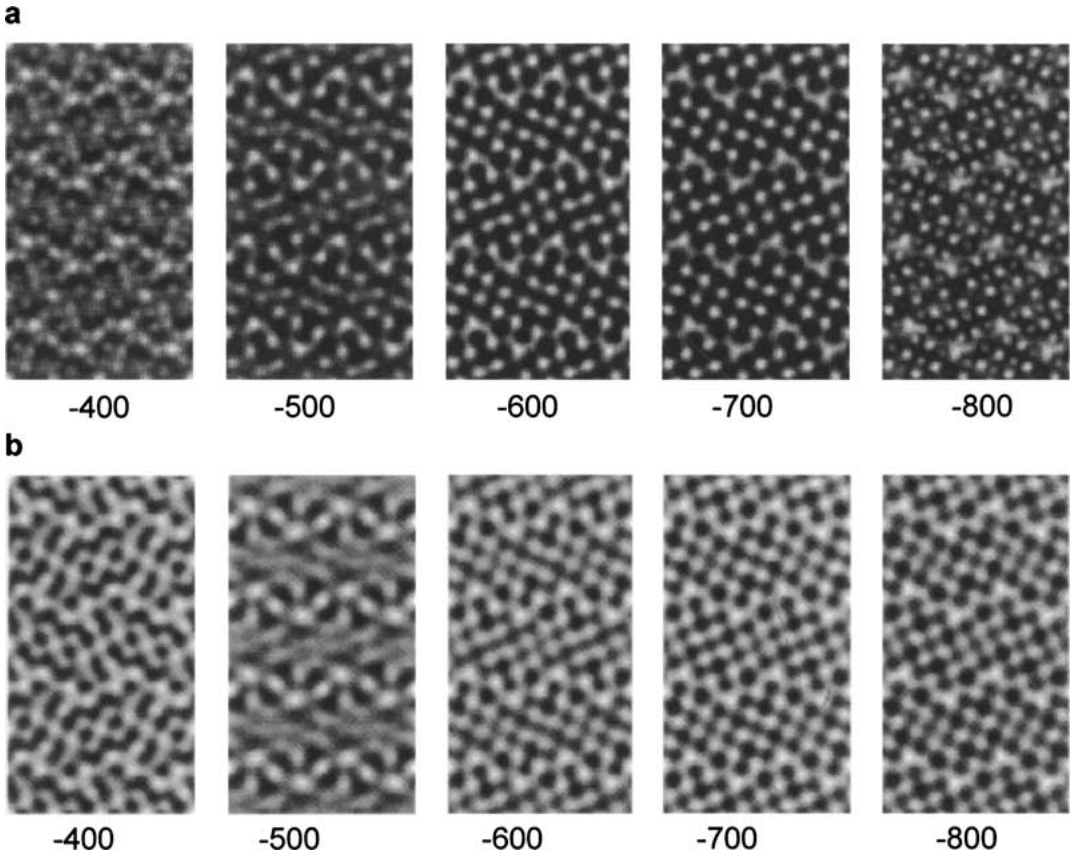

Figure 7 Computer simulated TEM images for $Ba_{4.5}Pr_9Ti_{18}O_{54}$ as a function of defocus of the objective lens for (a) a slice thickness of 53.49 Å, and (b) a slice thickness of 7.64 Å.

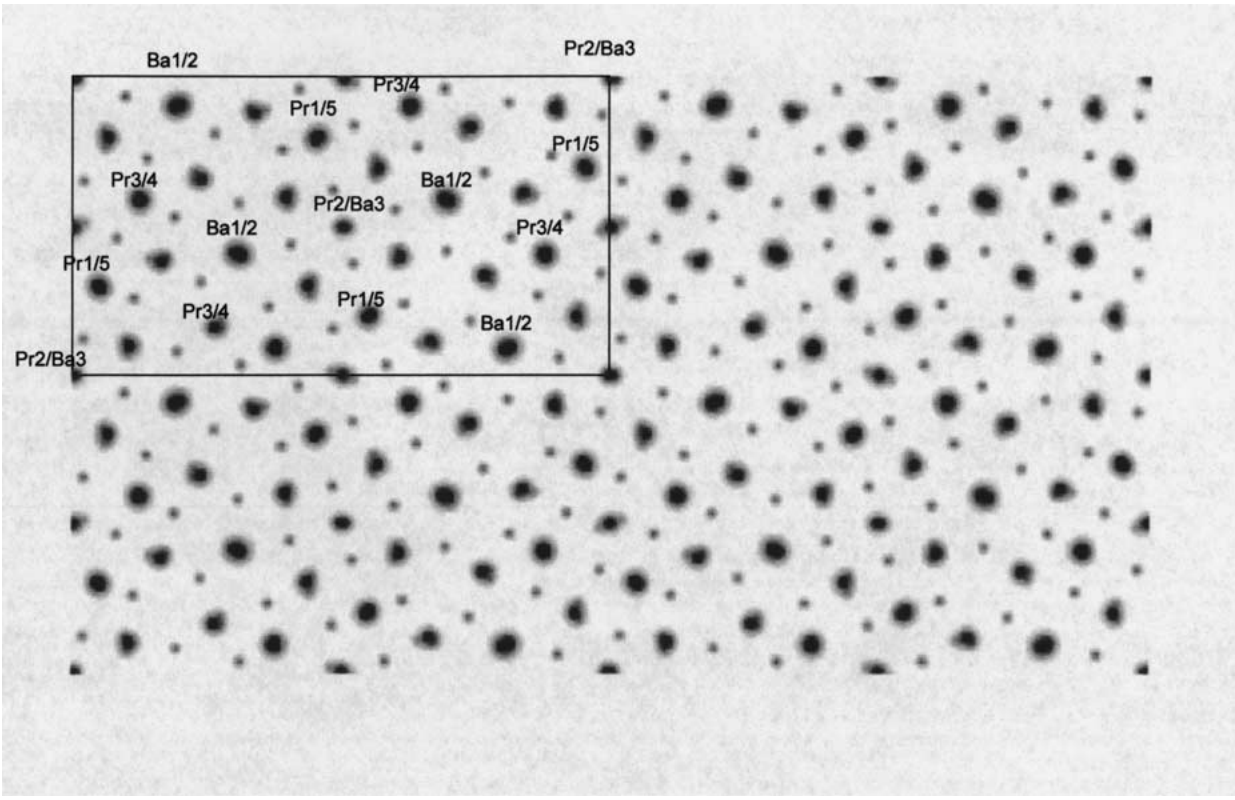

Figure 8 Projected potential (electron density) for $Ba_{4.5}Pr_9Ti_{18}O_{54}$ along [010].

projected potential (Fig. 8) to enable the Ba/Pr sites to be identified. In Fig. 9, the "best fit" simulated image (Fig. 9b; based on 2×2 unit cells) is superimposed on the experimental image (Fig. 9a); the inferred sites for Ba, for Pr, and Ba/Pr are highlighted within a single unit cell. This arrangement is consistent with space group pnam (No. 62) [1, 2, 9] and the structural model of Rawn *et al*. [2].

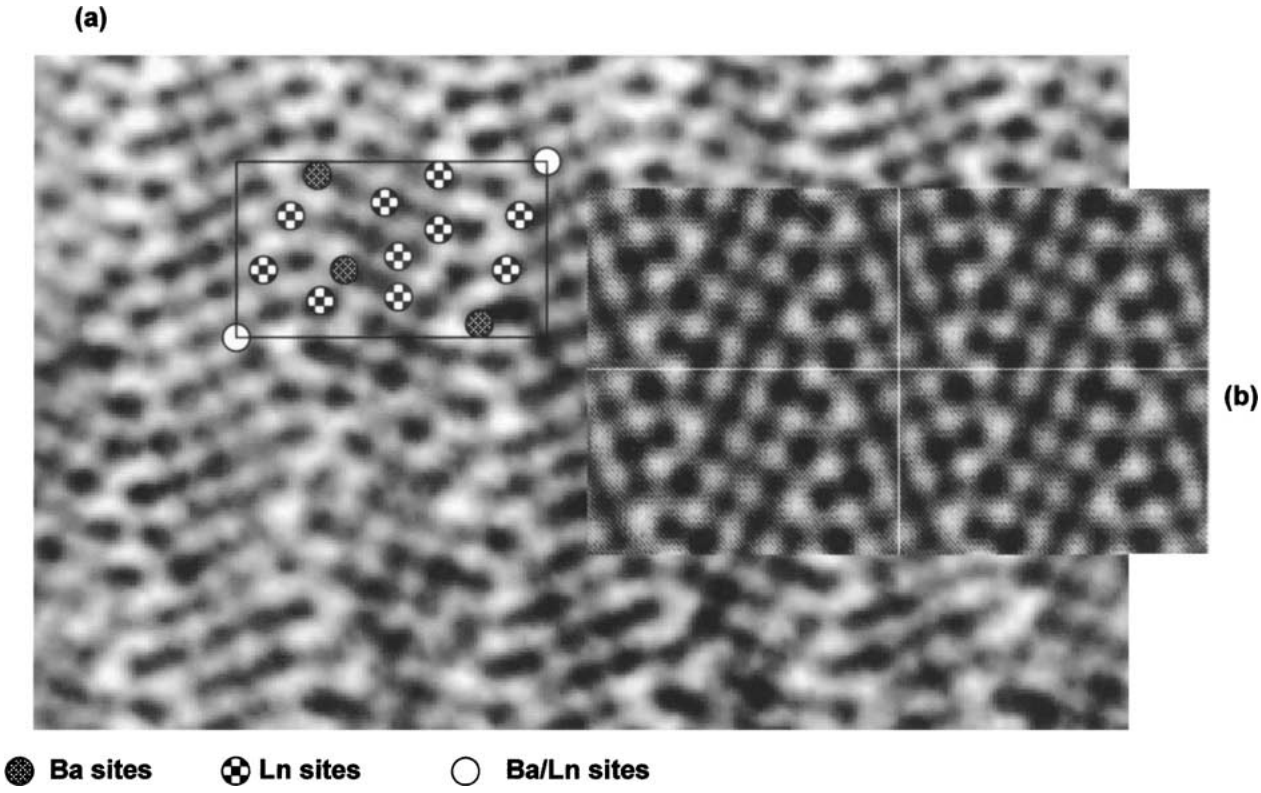

Figure 9 TEM images for $Ba_{4.5}Pr_9Ti_{18}O_{54}$ along [010] orientation: (a) experimental image, (b) simulated image (for 2×2 unit cells) for thickness of 1 unit cell and defocus of -700 Å is superimposed on top of experimental image (a). Note good match between (a) and (b). The inferred sites for Ba, Ln and Ba/Ln are highlighted within a single unit cell on the experimental image (a).

4. Conclusions

$Ba_{4.5}Pr_9Ti_{18}O_{54}$ has an orthorhombic crystal structure with a doubled unit cell in the shortest axis, possibly due to an order-disorder transformation. This idea is supported by the observation of anti-phase domain boundaries.

Simulation of TEM images were generated for a variety of crystal thicknesses. Good agreement was obtained with the experimental images for selected focus conditions. For $Ba_{4.5}Pr_9Ti_{18}O_{54}$, the results are consistent with the space group pnam (No. 62) [1, 2, 9] and the structural model of Rawn *et al* [2].

Acknowledgement

The support of the EPSRC through research grant GR/L33306 is gratefully acknowledged.

References

1. F. AZOUGH, P. E. CHAMPNESS and R. FREER, *J. Appl. Crystallogr.* **28** (1995) 557.
2. C. J. RAWN, D. P. BIRNIE III, M. A. BRUK, J. H. ENEMARK and R. S. ROTH, *J. Mater. Res.* **13** (1998) 187.
3. R. L. BOLTON, PhD Thesis, University of Illinois (Urbana, Illinois, USA, 1968)
4. D. KOLAR, Z. STADLER, S. GABRSCEK and D. SUVOROV, *Ber. Dtsch. Keram. Ges.* **55** (1978) 346.
5. K. WAKINO, K. MINAI and H. TAMURA, *J. Amer. Ceram. Soc.* **67** (1984) 278.
6. D. S. NISHIGAKI, H. KATO, S. YANO and R. KAMMURA, *Am. Ceram. Soc. Bull.* **66** (1987) 1405.
7. D. KOLAR, S. GABRSCEK and D. SUVOROV, in Proceedings of the Third European Ceramic Society Conference (Madrid 1993), edited by P. Duran and J. F. Fernandez (Faenza Editrice Iberica, 1993) Vol. 2, p. 229.
8. A. M. GENS, M. B. VARFOLOMEEV, V. S. KOSTOMAROV and S. S. KOROVIN, *Russ. J. Inorganic Chem.* **26** (1981) 482.
9. R. G. MATVEEVA, M. B. VARFOLOMEEV and L. S. IUYUSHEENKO, *Zh. Neorg. Khim.* **29** (1984) 17.
10. R. S. ROTH, F. BEACH, A. SANTORO, K. DAVIS, J. L. SOUBEYROUX and M. ZUCCHI, *Acta Cryst.* **A43** (1987) C138.
11. F. AZOUGH, P SETASUWON and R. FREER, in "Materials and Processes for Wireless Communications," edited by T. Negas and H. Ling (American Ceramic Society, Westerville, OH, 1995) p. 215.
12. H. OHSATO, S. NISHIGAKI and T. OKUDA, *Jpn. J. Appl. Phys.* **31** (1992) 3136.
13. C. J. RAWN, in Proceedings of Conference 'Electroceramics V', Aveiro, Portugal, 1996, Vol. 2 (University of Aveiro, 1996) p. 67.
14. H. OKUDERA, H. NAKAMURA, H. TORAYA and H. OHSATO, *J Solid State Chem.* **141** (1999) 336.
15. R. UBIC, I. M. REANEY and W. E. LEE, *J. Amer. Ceram. Soc.* **82** (1999) 1336.
16. H. OHSATO, A. KOMURA, Y. TAKAGI, S. NISHIGAKI and T. OKUDA, *Japanese J. Appl. Phys.* **37** (1998) 5357.
17. J. M. COWLEY and A. F. MOODIE, *Acta Cryst.* **10** (1957) 609.

Received 1 December 2000
and accepted 23 July 2001